Preprint typeset using LaTeX style emulateapj v. 5/2/11

arXiv:1206.5412v1 [astro-ph.CO] 23 Jun 2012

THE CORE-CUSP PROBLEM IN COLD DARK MATTER HALOS AND SUPERNOVA FEEDBACK: EFFECTS OF OSCILLATION

Go Ogiya and Masao Mori
Graduate School of Pure and Applied Science, University of Tsukuba, 1-1-1 Tennodai, Tsukuba 305-8577, Japan

ABSTRACT

We investigate the dynamical response of dark matter halos against recurrent starbursts in forming less-massive galaxies to solve the core-cusp problem, which is a discrepancy between the observation and the cold dark matter model. The gas heated by supernova feedbacks after a starburst expands, and then the star formation terminates. This expanding gas loses energy by radiative cooling, and then falls back toward the galactic center. Subsequently, a starburst arises again. This cycle of expansion and contraction of the interstellar gas leads to the recursive change in the gravitational potential of the interstellar gas. The resonance between dark matter particles and the density wave excited by the oscillating potential plays a key role to understand the physical mechanism of the cusp-core transition of dark matter halos. The dark matter halos effectively gain the kinetic energy from the energy transfer driven by the resonance between particles and the density waves. We find the critical condition for the cusp-core transition that the oscillation period of the gas potential should be approximately the same as the local dynamical time of the dark matter halo. We present the resultant core radius of the dark matter halo after the cusp-core transition induced by the resonance using the conventional mass-density profile predicted by the cold dark matter models. Moreover, we verified the analytical model using N-body simulations and the results nicely confirm the resonance model.

Subject headings: galaxies: dwarf — galaxies: halos — galaxies: kinematics and dynamics — galaxies: structure — galaxies: evolution

1. INTRODUCTION

Cold dark matter (CDM) cosmology, which is the standard paradigm of structure formation in the universe, contains several serious unsolved problems. Recent observations of nearby less-massive galaxies and low surface brightness galaxies have revealed that the density profile of the dark matter halo is constant at the center of these galaxies (e.g., Moore 1994; Burkert 1995; de Blok et al. 2001; Swaters et al. 2003; Weldrake et al. 2003; Gentile et al. 2004; Spekkens et al. 2005; Kuzio de Naray et al. 2006, 2008; Oh et al. 2008, 2011). However, in cosmological N-body simulations based on collisionless CDM, dark matter (DM) halos always have a steep power-law mass-density distribution at the center (e.g., Navarro et al. 1997; Fukushige & Makino 1997; Moore et al. 1998, 1999; Jing & Suto 2000; Klypin et al. 2001; Fukushige et al. 2004; Navarro et al. 2004; Diemand et al. 2004; Reed et al. 2005; Stadel et al. 2009; Navarro et al. 2010; Ishiyama et al. 2011). This discrepancy is a well-known unsolved problem in the CDM scenario and is so-called the “Core-Cusp problem”.

To solve this problem, this study has focused how baryon components gravitationally affect DM halos because less-massive galaxies like dwarf galaxies are more sensitive to stellar activity such as supernova explosions than giant ones owing to their shallow gravitational potential well. In dwarf galaxies, the hydrodynamic response against the stellar activity depends on the combination of various factors such as mass, morphology, and the star formation rate of the dwarf galaxies (e.g., Dekel & Silk 1986; Yoshii & Arimoto 1987; Mori et al. 1997, 1999, 2002; MacLow & Ferrara 1999; Silich & Tenorio-Tagle 2001, Bland-Hawthorn et al. 2011).

In less massive galaxies with a smooth gas distribution, supernova feedbacks blow the interstellar gas out from the galaxy centers. This mass loss reduces the depth of the gravitational potential around the center of DM halos and may flatten the central cusp of these halos. So far, the dynamical effects of this process on DM halos have been studied using collisionless N-body simulations (Navarro et al. 1996a; Gnedin & Zhao 2002; Read & Gilmore 2005; Ogiya & Mori 2011; Ragone-Figueroa et al. 2012). Ogiya & Mori (2011) have argued the relation between dynamical response of DM halos and timescale of mass loss (i.e. the star formation rate). The density profile of DM halos is correlated with the mass loss timescale and is flatter when mass loss occurs over a short time than that over a long time. However, even if mass loss occurs instantaneously, which is maximal effect, the central cusp remains; thus Ogiya & Mori (2011) conclude that the mass loss is not a prime mechanism to flatten the central cusp. When the mass loss timescale is much longer than the dynamical time of the system, the density profile of the DM halo recovers its initial cusp profile.

Massive galaxies with moderate stellar activity are more robust against supernova feedback, so supernovae can expel only small fraction of the gas from these galaxies. The gas heated by supernova feedbacks shortly after a burst of star formation expands temporarily, and then the star formation is terminated. The expanding gas loses energy by radiative cooling and then falls back toward the galactic center. Then, star formation will enhance again and ignite star burst subsequently (Stinson et al. 2007). This repetitive gas motion leads to the recursive change in the gravitational potential. Using hydrodynamic simulations combined with star formation and supernova feedback, the dynamical effects of such recurring changes have been studied (Governato

ogiya@ccs.tsukuba.ac.jp

et al. 2010; Pontzen & Governato 2012; Maccio' et al. 2012) and indicate that oscillations in the gravitational potential may modify the central cusp into a flat core. Read & Gilmore (2005) also argue the importance of recurring changes in the gravitational potential. The oscillation timescale is also an important factor in determining the dynamical effects on DM halos, and dwarf galaxies in the Local Group each have distinctive star formation histories (SFHs) (e.g., Mateo 1998; Tolstoy et al. 2009; McQuinn et al. 2010a, 2010b; Weisz et al. 2011). Furthermore, recurring star formation activities duplicates properties (e.g., metal distribution, and the velocity-dispersion profile) of dwarf spheroidal galaxies (Ikuta & Arimoto 2002; Marcolini et al. 2006, 2008). On the other hands, several other mechanisms have also been proposed to solve the Core-Cusp problem. Representative models involve the dynamical friction induced by the motion of gas or stellar clumps (Mashchenko et al. 2006, 2008; Inoue & Saitoh 2011) and bar instability (Weinberg & Katz 2002).

In this paper, we investigate the physical mechanism about the cusp-core transition under the recurring change in gravitational potential of the interstellar gas. Especially, we focus on the energy transfer driven by the resonance between DM particles and density waves induced by the oscillating gravitational potential. Then, we clarify the cusp-core transition of the DM halos using collisionless N-body simulations. This paper is structured as follows. Our analytic resonance model is described in §2. In §3, we present the result of our numerical simulations and interpret them with the aid of the resonance model. Finally, we summarize and discuss the results in §4.

2. ANALYTIC MODEL

The oscillation process (i.e. dynamical oscillation of gas in galactic potential) is an external force-like forced oscillation for DM halos. What is the dynamical response of DM halos to this force? To answer this question, we construct a simple analytic model to analyze the possibility of resonance between DM particles and density waves induced by the external baryon potential.

2.1. *Resonance model*

We approximate DM halo is treated as a fluid and the dynamical evolution of the system is described by the linearized fluid equations of the perturbed equilibrium state. Hereafter, we label physical quantities in the initial equilibrium state as “0”, external forces as “ex”, and induced quantities as “ind”. We assume infinite constant density field to as the equilibrium state ($\rho_0 = const.$), pick out a group of particles which have some constant velocity ($v_0 = const.$). In addition, the absolute values of the induced quantities are assumed to be much smaller than that of the equilibrium state or the external force. With these assumptions, the linearized equation of motion is given by,

$$\frac{\partial v_{\rm ind}(t,x)}{\partial t} + v_0 \frac{\partial v_{\rm ind}(t,x)}{\partial x} = -\frac{\partial \Phi_{\rm ex}(t,x)}{\partial x}, \qquad (1)$$

where the induced potential $\Phi_{\rm ind}$ is neglected.

Hereafter, we discuss the case in which the system is forced oscillation such as

$$-\frac{\partial \Phi_{\rm ex}}{\partial x} = A \sin{(kx - \Omega t)}, \qquad (2)$$

where A, k and Ω are the oscillation strength which is a positive constant, the wavenumber, and the angular frequency of the external force, respectively. The solution of Eq. (1) is given as follows,

$$v_{\rm ind}(t,x) = \frac{A}{\Omega - kv_0} \cos{(kx - \Omega t)}. \qquad (3)$$

The linearized equation of continuity can be similarly obtained,

$$\frac{\partial \rho_{\rm ind}(t,x)}{\partial t} + v_0 \frac{\partial \rho_{\rm ind}(t,x)}{\partial x} = -\rho_0 \frac{\partial v_{\rm ind}(t,x)}{\partial x}, \qquad (4)$$

and the solution is given by

$$\rho_{\rm ind}(t,x) = \frac{A\rho_0 k}{(\Omega - kv_0)^2} \cos{(kx - \Omega t)}. \qquad (5)$$

From these solutions, we notice that when $\Omega \to kv_0$, the coefficients diverge, and this is the resonant condition. Unfortunately, the signs of induced values are not able to be decided without the relations between Ω and kv_0, and the phase of the wave. Next, we consider the energy interchange between the DM collisionless system and the oscillatory external force.

In the following, we evaluate the change of the kinetic energy density of the particle group with the constant density ρ_0 and velocity v_0 in the equilibrium state. The kinetic energy density in the equilibrium state K_0 and after wobbled by the external force K are written by

$$K_0 = \frac{1}{2}\rho_0 v_0^2, \qquad (6)$$

$$K = \frac{1}{2}(\rho_0 + \rho_{\rm ind})(v_0^2 + 2v_0 v_{\rm ind} + v_{\rm ind}^2). \qquad (7)$$

Thus the change of the kinetic energy density, δK is

$$\delta K \equiv K - K_0 = \frac{1}{2}\rho_0(2v_0 v_{\rm ind} + v_{\rm ind}^2) + \frac{1}{2}\rho_{\rm ind}(v_0^2 + 2v_0 v_{\rm ind} + v_{\rm ind}^2). \qquad (8)$$

Averaging δK over a wavelength, we obtain the averaged change of the kinetic energy density,

$$< \delta K >= \frac{\rho_0 A^2}{4} \frac{\Omega + kv_0}{(\Omega - kv_0)^3}. \qquad (9)$$

From Eq. (9), when $\Omega - kv_0 > 0$, the particle group gains the kinetic energy from the external force. On the other hand, when $\Omega - kv_0 < 0$, its kinetic energy decreases.

Note that we have thus far confined the argument to a particular group of particles. Practically, the system have uncounted groups of particles, and each of them has respective densities and velocities in the equilibrium state. In the realistic self-gravitational systems, particles having low energy (i.e. low velocity) are more dominated than particles having high velocity. Thus, the change of the kinetic energy density overall the system, ΔK will be positive, i.e.,

$$\Delta K \equiv \int < \delta K > d\rho_0 dv_0 > 0. \qquad (10)$$

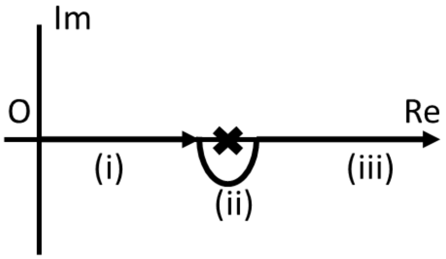

FIG. 1.— The integration path. The cross symbol shows the singular point, $v = \Omega/k$. We separate the contour into three parts, (i), (ii), and (iii).

From Eq. (10), we know the system gains the kinetic energy from the external force substantively, and it will expand. In other words, $v_{\rm ind} > 0$ and $\rho_{\rm ind} < 0$ for the whole of the system.

As an example, we assume Maxwell-Boltzmann distribution for particle velocity and evaluate the change of kinetic energy density overall the system, $\Delta K \propto \int_0^\infty dv < \delta K(v) > e^{-v^2} \equiv \int_0^\infty dv f(v)$. To avoid the singular point of $< \delta K(v) >$ (i.e., $v = \Omega/k$) we change the integration path as shown in Fig.1. The value of the integration is conserved through this change. The integration can be separated into three parts,

$$\Delta K \propto \int_0^\infty dv f(v) = \int_{\rm (i)} dv f(v) + \int_{\rm (ii)} dv f(v) + \int_{\rm (iii)} dv f(v). \quad (11)$$

We can evaluate the second term using the residue theorem, and we find the second term is an imaginary number. We ignore it. The first and the third are positive and negative, since $\Omega - kv > 0$ and $\Omega - kv < 0$ is satisfied, respectively. The absolute value of the third term will be smaller than the first term, because it is damped by Gaussian strongly. Thus, ΔK will be positive, i.e. the system gains kinetic energy from the external force substantively, and it will expand. In other words, $v_{\rm ind} > 0$ and $\rho_{\rm ind} < 0$ for the whole of the system.

According to the above argument, we conclude that the particles gain the kinetic energy effectively, if the particles satisfy the resonance condition,

$$kv \approx \Omega. \quad (12)$$

Therefore, the system will expand to settle new equilibrium state, and the density will decrease.

2.2. *Resonance condition*

In this section, we apply the resonance condition to a spherical system and simply extend it as follows,

$$k(r)\sigma(r) \approx \Omega, \quad (13)$$

where r is the distance from the center of the system, the wave number, $k(r)$ as a function of r is defined by

$$k(r) \equiv \frac{2\pi}{r}. \quad (14)$$

Assuming the virial theorem, v_0 in Eq. (12) is substituted by the velocity dispersion

$$\sigma(r) = \sqrt{\frac{GM(r)}{r}}, \quad (15)$$

where $M(r)$ is mass within r. Here, we define the dynamical time of the system as

$$t_{\rm d}(r) = \sqrt{\frac{3\pi}{32G\bar{\rho}(r)}}, \quad (16)$$

where

$$\bar{\rho}(r) = \frac{M(r)}{(4\pi/3)r^3}, \quad (17)$$

is the average density interior to radius r. In this case, the resonance condition in Eq. (13) becomes

$$t_{\rm d}(r) = \frac{\pi}{2\sqrt{2}}T \sim T, \quad (18)$$

where $T \equiv 2\pi/\Omega$ is the oscillation period.

Furthermore, we consider the resonances of the overtone modes. Hereafter, "1" denotes the fundamental-tone, and "n" denotes n-th overtone ($n = 2, 3, \cdots$). The resonance scale of the fundamental-tone is $r_1 \equiv 2\pi/k_1$, thus those of the overtones are

$$r_n = 2\pi/k_n = 2\pi/nk_1 = r_1/n. \quad (19)$$

The resonance condition for the n-th overtone is $t_{\rm d}(r_n) \sim T/n$. According to this argument, the resonance scale will be nearly equal to r_1 for which the resonance condition,

$$t_{\rm d}(r_1) \sim T, \quad (20)$$

is satisfied. From this equation, we can derive the resonant radius using the inversion procedure

$$r_1 = t_d^{-1}(T). \quad (21)$$

The resonance of the overtone modes will occur in the central dense region of the DM halo and the resonance of the fundamental-tone will appear in the outer less dense region. In the next section, we apply this argument to the models of CDM halos predicted by cosmological N-body simulations, Eq. (22) and estimate the core scale.

2.3. *Core scale*

The mass-density profile of a DM halo obtained from cosmological N-body simulations based on the CDM scenario can be fitted by the following formula:

$$\rho_{\rm DM}(x) = \frac{\rho_0}{x^\alpha (x+1)^{3-\alpha}}, \quad (22)$$

where $x \equiv r/R_{\rm DM}$, r is the distance from the center of the DM halo, α is a power-law index of the central cusp, and ρ_0 and $R_{\rm DM}$ are the scale density and scale length of a DM halo, respectively. This formula indicates that the density distribution of a DM halo changes from $\rho \propto r^{-\alpha}$ in the center ($r < R_{\rm DM}$) to $\rho \propto r^{-3}$ at the outskirts ($r > R_{\rm DM}$). Here, $\alpha = 1.0$ corresponds to the Navarro–Frenk–White (NFW) model (Navarro et al. 1996b; Navarro et al. 1997) and $\alpha = 1.5$ is similar to the Fukushige–Makino–Moore (FMM) model (Fukushige & Makino 1997; Moore et al. 1999).

The mass profile derived by Eq. (22) is given by

$$M(\alpha;x)=\frac{4\pi\rho_0 R_{\rm DM}^3}{3-\alpha}x^{3-\alpha}\ {}_2F_1[3-\alpha,3-\alpha,4-\alpha;-x], \tag{23}$$

where ${}_2F_1[3-\alpha,3-\alpha,4-\alpha;-x]$ is Gauss's hypergeometric function, which we denote hereafter simply by ${}_2F_1$ $[\alpha;-x]$. From Eq.(23),

$$\rho_0=\frac{3-\alpha}{4\pi R_{\rm DM}^3}\frac{1}{c^{3-\alpha}{}_2F_1[\alpha;-c]}M_{\rm vir}. \tag{24}$$

where the virial mass of a DM halo is defined by

$$M_{\rm vir}=\frac{4\pi}{3}\rho_{\rm cri}(1+z)^3\Delta R_{\rm vir}^3, \tag{25}$$

where $\rho_{\rm cri}$ is the critical density of the universe, z is redshift, $\Delta(=200)$ is a parameter of the density enhancement, $c=R_{\rm vir}/R_{\rm DM}$ is a concentration parameter, and $R_{\rm vir}$ is a virial radius.

Using Eqs. (23) and (24), the average density of the DM halo interior to radius x is given by

$$\bar{\rho}(x)=\frac{3M_{\rm vir}}{4\pi R_{\rm DM}^3}\frac{x^{-\alpha}}{c^{3-\alpha}}\frac{{}_2F_1[\alpha;-x]}{{}_2F_1[\alpha;-c]}, \tag{26}$$

and by using the resonance condition given in Eq. (20), we finally arrive at the core scale $r_{\rm core}=x_{\rm core}\,R_{\rm DM}$.

We now discuss the utmost limit, $x_{\rm core}\ll 1$. When $x_{\rm core}\ll 1$, the approximation ${}_2F_1[\alpha;-x]\sim 1$ holds. Thus, the core scale is expressed as

$$r_{\rm core}=R_{\rm DM}\left[\frac{8G}{\pi^2}\frac{M_{\rm vir}T^2}{R_{\rm DM}^3 c^{3-\alpha}{}_2F_1[\alpha;-c]}\right]^{1/\alpha}, \tag{27}$$

$$=R_{\rm DM}\left[\frac{32G}{3\pi}\Delta\rho_{\rm cri}(1+z)^3\frac{c^{\alpha}}{{}_2F_1[\alpha;-c]}T^2\right]^{1/\alpha}. \tag{28}$$

Using Eq. (25), we obtain more convenient formulae for NFW model ($\alpha=1.0$) and FMM model ($\alpha=1.5$). The general formulae are given by

$$r_{\rm core}=0.74\ {}_2F_1[1;-c]^{-1}(1+z)^2\Big(\frac{M_{\rm vir}}{10^9M_\odot}\Big)^{1/3}\Big(\frac{T}{10^7{\rm yr}}\Big)^2{\rm pc}, \tag{29}$$

for the NFW model, and

$$r_{\rm core}=23\ {}_2F_1[1.5;-c]^{-2/3}(1+z)\Big(\frac{M_{\rm vir}}{10^9M_\odot}\Big)^{1/3}\Big(\frac{T}{10^7{\rm yr}}\Big)^{4/3}{\rm pc}, \tag{30}$$

for the FMM model. Here, we show some values of ${}_2F_1[\alpha;-c]$ in Table 1 for $\alpha=1.0,1.5$ and some ordinary c parameters obtained from cosmological N-body simulations (e.g., Maccio' et al. 2008). When we assume $c=10$ and $z=0$, we reach the core scale by following simpler formulae:

$$r_{\rm core}=25\ \Big(\frac{M_{\rm vir}}{10^9M_\odot}\Big)^{1/3}\Big(\frac{T}{10^7{\rm yr}}\Big)^2{\rm pc}, \tag{31}$$

for the NFW model, and

$$r_{\rm core}=120\ \Big(\frac{M_{\rm vir}}{10^9M_\odot}\Big)^{1/3}\Big(\frac{T}{10^7{\rm yr}}\Big)^{4/3}{\rm pc}, \tag{32}$$

for the FMM model.

In the next section, we compare our analytic prediction with the results of N-body simulations.

TABLE 1
NUMERICAL VALUES OF ${}_2F_1[\alpha;-c]$ FOR CONVENTIONAL MODELS OF DM HALOS

α (Model)	$c=5$	$c=10$	$c=15$	$c=20$
1.0 (NFW)	0.07667	0.02978	0.01631	0.01046
1.5 (FMM)	0.16948	0.08681	0.05656	0.04117

NOTE. — α is the power-law index of the central cusp of a DM halo and c is the concentration parameter.

3. NUMERICAL SIMULATIONS

3.1. *Numerical models*

In this section, we describe our collisionless N-body simulations. To generate N-body systems with a cusp described in Eq. (22), in the equilibrium state, we use the fitting formulation of the distribution function (DF) proposed by Widrow (2000). In this case, the DF only depends on energy, thus the velocity dispersion of the system is isotropic.

We adopt the Hernquist potential (Hernquist 1990) to describe the baryon potential around the center of the DM halos. The external potential is given by

$$\Phi_{\rm b}(r,t)=-\frac{GM_{\rm b}}{r+R_{\rm b}(t)}, \tag{33}$$

where $M_{\rm b}$ and $R_{\rm b}(t)$ are total baryon mass and scale length of the external potential, respectively. We change the scale length of the baryon potential to $R_{\rm b}(t)=0.5[R_{\rm b,max}-R_{\rm b,min}][1+\cos{(\Omega t)}]+R_{\rm b,min}$, where $\Omega\equiv 2\pi/T$, T is the timescale of oscillation of the external potential, $R_{\rm b,max}$ and $R_{\rm b,min}$ are maximum and minimum scale length, respectively.

To construct a stable initial condition, we dynamically relax the equilibrium N-body system quoted above in the external baryon potential with the fixed scale length $R_{\rm b}=R_{\rm b,max}$ to $\sim 30\ t_{\rm d}(0.2)$, where $t_{\rm d}(0.2)$ is the dynamical time defined by Eq. (16) at $r=0.2$ kpc. The resultant density profiles are almost the same as the initial non-perturbed system of NFW and FMM model.

In this study, we simulate the dynamical response of a DM halo with virial mass $M_{\rm vir}=10^9M_\odot$, the virial radius $R_{\rm vir}=10$ kpc, the scale length $R_{\rm DM}=2$ kpc, and we assume $z=1$. In this case, the mean dynamical time within 0.2 kpc is $t_{\rm d}(0.2)=4$ Myr for the FMM model and 10 Myr for the NFW model. Other parameters adopted in each of our simulation runs are shown in Table 2. Throughout this paper, the total number of particles is $N=1,048,576$, the tolerance parameter of the Barnes–Hut tree algorithm (Barnes & Hut 1986) is $\theta=0.8$ and the softening parameter is $\epsilon=0.008$ kpc.

3.2. *Results*

In this section, we present the results of our N-body simulations and compare them with the theoretical prediction via the simple analytic model given in §2.

Figure 2 shows the distribution function of DM particles as a function of the radial velocity. Dashed line is the equilibrium (non-perturbed) state of the N-body system for FMM model. Before adding the oscillatory external potential, we generate an initial stable N-body system with a fixed external baryon potential for a constant scale length $R_{\rm b}(t)=R_{\rm b,max}$ defined by Eq. (33). Thin dotted line corresponds the distribution function of

DM particles at $15t_{\rm d}(0.2)$. After $30t_{\rm d}(0.2)$, the system reached the quasi-stable state, and it remains virtually unchanged (thick dotted line). Then, we add the oscillatory external potential given by Eq. (33). Solid line corresponds the distribution function with the system after several oscillations. It clearly shows that the number of low-velocity particles decreases and that of high-velocity particles increases. This indicates that the system gains the net energy through the acceleration of the slow particles by the density waves induced by the oscillatory baryon potential.

TABLE 2
SUMMARY OF SIMULATION RUNS

ID	T [$t_{\rm d}$]	$M_{\rm b}$ [$\times 10^8 M_\odot$]	$R_{\rm b,max}$ [kpc]	$R_{\rm b,min}$ [kpc]
FMM1	1	1.7	2.0	0.04
FMM2	3	1.7	2.0	0.04
FMM3	10	1.7	2.0	0.04
FMM4	0.1	1.7	2.0	0.04
FMM5	50	1.7	2.0	0.04
FMM6	3	1.7	1.0	0.04
FMM7	3	1.7	2.0	0.1
FMM8	3	1.0	2.0	0.04
NFW1	1	1.7	2.0	0.04
NFW2	3	1.7	2.0	0.04
NFW3	10	1.7	2.0	0.04

NOTE. — FMM and NFW indicate initial DM halo model. T, $M_{\rm b}$, $R_{\rm b,max}$ and $R_{\rm b,min}$ are the period of oscillation, the total mass, and the maximum and the minimum scale length of the external baryon potential, respectively. We adopt the mass ratio of baryon component to a DM halo cosmic value obtained from *Wilkinson Microwave Anisotropy Probe* observations (Spergel et al. 2007; Komatsu et al. 2009, 2011).

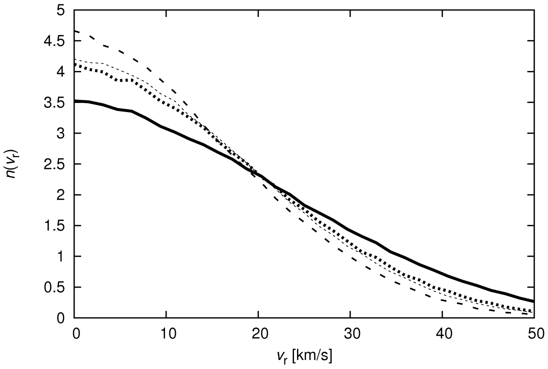

FIG. 2.— Distribution functions of DM particles for FMM model as a function of the radial velocity. Dashed line is the equilibrium (non-perturbed) state. Thin-dotted line (thick-dotted line) is for $t = 15t_{\rm d}(0.2)$ ($t = 30t_{\rm d}(0.2)$) after adding the oscillatory external potential with a fixed external baryon potential for a constant scale length $R_{\rm b}(t) = R_{\rm b,max}$ defined by Eq. (33). Solid line corresponds the distribution function for the quasi-equilibrium state after several oscillations.

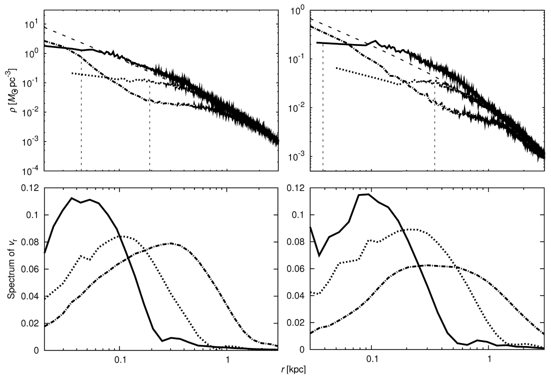

FIG. 3.— Density profile (top panels) and spectrum of radial velocity (bottom panels) of the DM halos after several oscillations of the external potential. Left panels are results of FMM model (FMM1, FMM2 and FMM3), and right panels are NFW model (NFW1, NFW2 and NFW3). Solid, dotted, dot-dashed, and dashed lines represent $T = 1, 3, \text{and} 10 t_{\rm d}$ and the initial condition, respectively. Each vertical line is the core scale predicted by Eq. (29) and (30).

Figure 3 demonstrates how the dynamical response of DM halos depends on the oscillation frequency of the external baryon potential. In each panel, solid, dotted, dot-dashed and dashed lines correspond to $T = 1, 3$ and $10\,t_{\rm d}(0.2)$ and the initial condition, respectively. The upper-left (upper-right) panel corresponds the final density profiles of DM halos for initially FMM (NFW) model after several oscillation periods. All of the models clearly show the cusp-core transition and the resultant core scale depends on the oscillation frequency of the external baryon potential. The vertical dashed lines in both panels correspond the core scale predicted by Eq. (29) or (30), where the left and right lines are the cases for $T = t_{\rm d}(0.2)$ and $T = 3\,t_{\rm d}(0.2)$, respectively. As you can see, our analytic model perfectly predicts the core scale derived by these numerical experiments. On the other hand, the system evolves adiabatically for the slow oscillation with $T = 10\,t_{\rm d}(0.2)$. In this case of the adiabatic change in potential, the system always accommodates the potential, and the central cusp remains (Ogiya & Mori 2011). Although the central cusp is remains, however, a bump appears at the outskirts of the DM halo. This bump is obviously generated by the resonance of the density wave. Despite beyond the appropriate range of the approximation $x_{\rm core} \ll 1$, Eq. (30) gives a reasonable prediction such as $r_{\rm core} = 0.95$ kpc for FMM halo.

Here, we compute the Fourier transform of the radial velocity of the systems as a function of r using each snapshot of data to verify the emergence of the energy transfer due to the resonance between the particles and the density waves. In the lower panels of Fig. 3, we show the Fourier components of the radial velocity of the angular frequency, ω, equal to the oscillation frequency of the external potential Ω. As you can see, there are the peaks accord with the core scale in the density profile, and the position of these peaks depends on T. We have demonstrated the spectrum of the fundamental mode for each run. These results clearly show that, as expected, the core scale agrees with the position of the peak predicted by Eq. (20). As we discussed in the previous section, the resonance of the slow oscillation appears at outer low-dense regions of DM halo, whereas that of the rapid oscillation appears at the inner more dense regions. This result indicates that when DM halos are in resonance with the external potential, they effectively accelerate particles, so that the core is created around the position of the peak.

Figure 4 shows the spatial distribution of the Fourier components of the radial velocity including the case of $\omega \neq \Omega$. Although we only show the results of the FMM model in this figure, a similar phenomenon appears for the NFW model. In the bottom panels of Fig. 3, we only show the fundamental mode for each T. Figure 4 clears up the resonance of overtone modes. For exam-

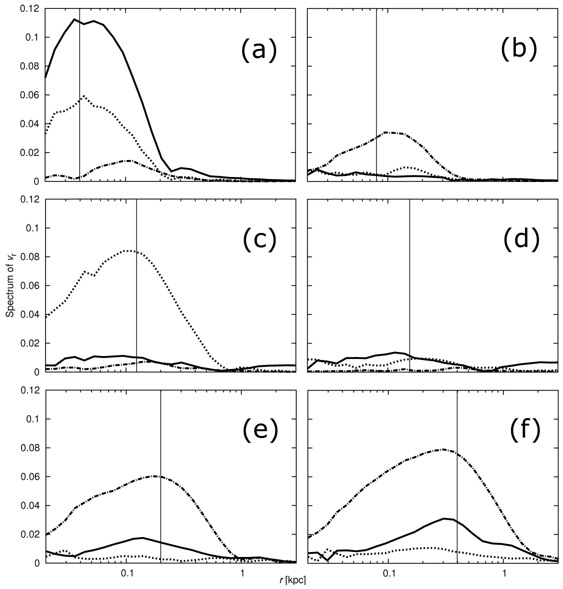

FIG. 4.— Spectrum of radial velocity of the DM halos (FMM1, FMM2 and FMM3). Each line represents the same for Fig. 3 and each panel corresponds for (a) $T = t_\mathrm{d}$, (b) $T = 2t_\mathrm{d}$, (c) $T = 3t_\mathrm{d}$, (d) $T = 4t_\mathrm{d}$, (e) $T = 5t_\mathrm{d}$, and (f) $T = 10t_\mathrm{d}$. Vertical lines show the predicted resonance scale, r_n. We consider the fundamental mode to correspond to $T = 10t_\mathrm{d}$ (viz. $\omega_1 = 2\pi/10t_\mathrm{d}$).

ple, the dot-dashed line, $T = 10t_\mathrm{d}(0.2)$, exhibits peaks in panels (f), (e), (b), and (a). These peaks correspond to the resonance of the fundamental mode and overtone modes $n = 2, 5$ and 10, respectively. Furthermore, vertical lines indicate the resonance scale between the fundamental mode and the overtone modes predicted by Eq. (19). If we can measure a resonant scale, then we can predict other resonance scales using this relation.

Figure 5 shows the resultant density profiles of the FMM model for the cases of the extremely rapid oscillation (model of FMM4) and the extremely slow oscillation (model of FMM5). Dotted line and thin solid line represent $T = 0.1t_\mathrm{d}(0.2)$ and $50t_\mathrm{d}(0.2)$, respectively. Dashed line is the initial condition, and dot-dashed line expresses the maximum-contracted case with $R_b(t) = 0.04$ kpc using the adiabatic contraction model argued in Blumenthal et al. (1986). For the rapid oscillation model, the DM particles are not able to respond the rapid change of the external potential. Therefore, the energy exchange between the density waves and the DM particles is inefficient, and the central cusp remains. In other words, this is limited by a numerical resolution. In the high-resolution simulations, the resonance will appear at the central region because the resonance is a scale-free. It should be noted that DM particles are exposed to some fixed external potential (see dotted line at the center), the DM halo concentrates more than the initial FMM model, and the degree of concentration is weaker than that for the maximum contraction case (dot-dashed line). The solid line corresponds the nearly adiabatic change in the gravitational potential. In this case, as discussed by Ogiya & Mori (2011), the system always accommodates the changing potential, and the central cusp remains, although there seems to be a bump in the mass density in the outskirts. The scale of the bump is nearly five times that for $T = 10t_\mathrm{d}$ (cf. Fig. 3).

Figure 6 demonstrates how the dynamical response of DM halos depends on the other parameters ($M_\mathrm{b}, R_\mathrm{b,max}$ and $R_\mathrm{b,min}$). The thin solid line is the initial condition of the FMM model. Thick solid, dotted, dot-dashed and dashed lines represent the resultant density profile of the model of FMM2, FMM6, FMM7, and FMM8, respectively. It is apparent that the resultant core scale is almost alike for each model, and the final density profile of the simulation is quite similar. Our results show that these parameters affect the number of oscillations needed to reach quasi-equilibrium state with the central core, but there is almost no effect on the final state of DM halos. This indicates that the period of oscillation is the most important parameter to determine whether the central cusp is flattened, and the core scale.

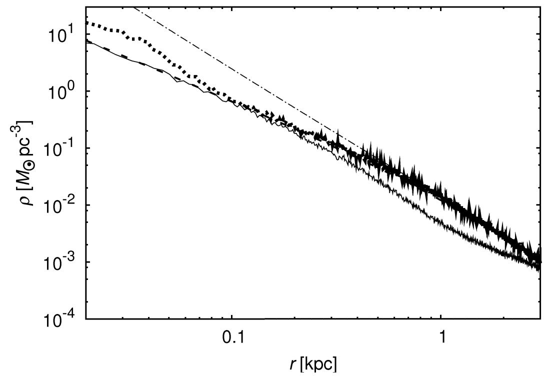

FIG. 5.— Density profile of the DM halos after oscillations of the external potential. Dashed line is the initial condition of the FMM model. Dotted line and thin-solid line represent $T = 0.1t_\mathrm{d}$ (FMM4) and $T = 50t_\mathrm{d}$ (FMM5), respectively. The dot-dashed line expresses the maximum-contracted case $R_b(t) = 0.04$kpc using the adiabatic contraction discussed by Blumenthal et al. (1986).

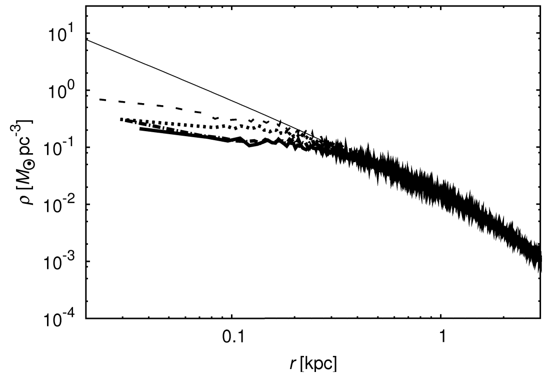

FIG. 6.— Density profile of the DM halos after oscillations of the external potential. The thin solid line is the initial condition, FMM model. Thick solid, dotted, dot-dashed, and dashed lines represent the result of FMM2, FMM6, FMM7, and FMM8, respectively.

4. SUMMARY AND DISCUSSION

We have studied the dynamical response of DM halos to recurring changes of the gravitational potential of the interstellar gas around the center of the DM halos. The resonance model between particles and the oscillating external potential is proposed to understand the physical mechanism of the cusp-core transition of DM halos. It is found that the collisionless system effectively gains the kinetic energy from the energy transfer driven by the resonance between DM particles and density waves induced by the oscillation of the gravitational potential of the

TABLE 3
COMPARISON WITH OBSERVATIONAL RESULTS

Galaxy	$r_{\rm core}$ [kpc]	$\rho(r_{\rm core})$ [$M_\odot {\rm pc}^{-3}$]	$t_{\rm d}(r_{\rm core})$ [Myr]	$\tau_{\rm SF}$ [Myr]
NGC 2366	0.6	0.05	40	~ 100
NGC 6822	1	0.03	50	~ 100
Holmberg II	0.5	0.03	50	~ 100

NOTE. — Approximated values of NGC 2366, NGC 6822, and Holmberg II. $r_{\rm core}$ is observed core radius, $\rho(r_{\rm core})$ is mass-density at $r_{\rm core}$, respectively. We obtained these values from Weldrake et al. (2003; NGC 6822), and Oh et al. (2008, 2011; NGC 2366, Holmberg II). We estimated the dynamical time at $r_{\rm core}$, $t_{\rm d}(r_{\rm core})$ using Eq. (16). $\tau_{\rm SF}$ is the interval of star formation in these galaxies, obtained from McQuinn et al. (2010a, 2010b).

interstellar gas. The condition for the cusp-core transition is that the oscillation period of the baryon potential should be approximately the same as the local dynamical time. In other words, the resonance condition at r is represented by $t_{\rm d}(r_{\rm core}) = T$ and the overtone modes are also in the resonant states. In addition, the core radius of the DM halo after the cusp-core transition driven by the resonance between particles and the density waves is shown using the conventional mass-density profile of DM halos, which is predicted by the cosmological structure formation models. Moreover, we verified our analytical model using N-body simulations and the simulation results nicely confirm our resonance model. Therefore, we conclude that the resonance between the DM particles and the oscillation of the baryon potential plays a key role in the cusp-core problem of DM halos.

Pontzen & Governato (2012) have a similar approach to understand how recurring potential flatten out the cusp of DM halos. They have studied about two limited cases in which potential changes instantaneously or adiabatically, and found that most particles in the system gain energy when potential change occurs instantaneously, and systems expand. As seen from above, our resonance model gives broad understanding of the fundamental physical mechanism of the cusp-core transition of DM halos. In addition, the model is able to predict the core scale quite precisely.

The oscillation of gas is directly correlated with the stellar activity of galaxies. In recent years, SFH and the density profile of nearby dwarf galaxies have been studied precisely. Our results imply that these two phenomena are correlated. For example, we adduce three galaxies; NGC 2366, NGC 6822, and Holmberg II (Table 3), which have a core structure at the center (Weldrake et al. 2003; Oh et al. 2008, 2011) and episodic SFHs (McQuinn et al. 2010a, 2010b). Their dynamical time at the core scale corresponds approximately to the interval of their episodic star formation activity. These galaxies conceivably justify the resonance condition predicted by Eq. (20) at the core scale. Yoshii & Arimoto (1991) have studied the color change of galaxies with oscillating star formation history. They revealed that the colors of galaxies also change oscillatory and that star formation activity imprints its record, depending on the initial mass function and oscillation period, in the two-color diagram. Evidence of oscillating SFHs may be detected, and the oscillation period might be measured more precisely in the future observations.

In the series of subsequent studies, we will examine a more realistic model that includes non-spherical analysis and gas dynamics and that will more closely study the correlation between density structure and the SFH of dwarf galaxies.

We would like to thank T. Okamoto, and A. Wagner for useful comments. Numerical simulations were performed with the FIRST simulator and T2K-Tsukuba at the Center for Computational Sciences at the University of Tsukuba. This work was supported in part by JSPS Grants-in-Aid for Scientific Research: (A) (21244013), (C) (18540242), and (S) (20224002), and Grants-in-Aid for Specially Promoted Research by MEXT (16002003).

REFERENCES

Babul, A., & Rees, M. J. 1992, MNRAS, 255, 346

Barnes, J., & Hut, P. 1986, Nature, 324, 446

Bland-Hawthorn, J., Sutherland, R., & Karlsson, T. 2011, EAS Publications Series, 48, 397

Blumenthal, G. R., Faber, S. M., Flores, R., & Primack, J. R. 1986, ApJ, 301, 27

Burkert, A. 1995, ApJ, 447, L25

de Blok, W. J. G., McGaugh, S. S., & Rubin, V. C. 2001, AJ, 122, 2396

Dekel, A., & Silk, J. 1986, ApJ, 303, 39

Diemand, J., Moore, B., & Stadel, J. 2004, MNRAS, 353, 624

Fukushige, T., & Makino, J. 1997, ApJ, 477, L9

Fukushige, T., Kawai, A., & Makino, J. 2004, ApJ, 606, 625

Gentile, G., Salucci, P., Klein, U., Vergani, D., & Kalberla, P. 2004, MNRAS, 351, 903

Gnedin, O. Y., & Zhao, H. 2002, MNRAS, 333, 299

Governato, F., Brook, C., Mayer, L., et al. 2010, Nature, 463, 203

Hernquist, L. 1990, ApJ, 356, 359

Ikuta, C., & Arimoto, N. 2002, A&A, 391, 55

Inoue, S., & Saitoh, T. R. 2011, MNRAS, 418, 2527

Ishiyama, T., Makino, J., Portegies Zwart, S., et al. 2011, arXiv:1101.202

Jing, Y. P., & Suto, Y. 2000, ApJ, 529, L69

Klypin, A., Kravtsov, A. V., Bullock, J. S., & Primack, J. R. 2001, ApJ, 554, 903

Komatsu, E., Dunkley, J., Nolta, M. R., et al. 2009, ApJS, 180, 330

Komatsu, E., Smith, K. M., Dunkley, J., et al. 2011, ApJS, 192, 18

Kuzio de Naray, R., McGaugh, S. S., de Blok, W. J. G., & Bosma, A. 2006, ApJS, 165, 461

Kuzio de Naray, R., McGaugh, S. S., & de Blok, W. J. G. 2008, ApJ, 676, 920

Macciò, A. V., Stinson, G., Brook, C. B., et al. 2012, ApJ, 744, L9

Mac Low, M.-M., & Ferrara, A. 1999, ApJ, 513, 142

Marcolini, A., D'Ercole, A., Brighenti, F., & Recchi, S. 2006, MNRAS, 371, 643

Marcolini, A., D'Ercole, A., Battaglia, G., & Gibson, B. K. 2008, MNRAS, 386, 2173

Mashchenko, S., Couchman, H. M. P., & Wadsley, J. 2006, Nature, 442, 539

Mashchenko, S., Wadsley, J., & Couchman, H. M. P. 2008, Science, 319, 174

Mateo, M. L. 1998, ARA&A, 36, 435

McQuinn, K. B. W., Skillman, E. D., Cannon, J. M., et al. 2010a, ApJ, 721, 297

McQuinn, K. B. W., Skillman, E. D., Cannon, J. M., et al. 2010b, ApJ, 724, 49

Mori, M., Yoshii, Y., Tsujimoto, T., & Nomoto, K., 1997, ApJ,

Mori, M., Yoshii, Y., & Nomoto, K., 1999, ApJ,

Mori, M., Ferrara, A., & Madau, P., 2002, ApJ,

Moore, B. 1994, Nature, 370, 629

Moore, B., Governato, F., Quinn, T., Stadel, J., & Lake, G. 1998, ApJ, 499, L5

Moore, B., Quinn, T., Governato, F., Stadel, J., & Lake, G. 1999, MNRAS, 310, 1147

Navarro, J. F., Eke, V. R., & Frenk, C. S. 1996a, MNRAS, 283, L72

Navarro, J. F., Frenk, C. S., & White, S. D. M. 1996b, ApJ, 462, 563

Navarro, J. F., Frenk, C. S., & White, S. D. M. 1997, ApJ, 490, 493

Navarro, J. F., Hayashi, E., Power, C., et al. 2004, MNRAS, 349, 1039

Navarro, J. F., Ludlow, A., Springel, V., et al. 2010, MNRAS, 402, 21

Ogiya, G., & Mori, M. 2011, ApJ, 736, L2

Oh, S.-H., de Blok, W. J. G., Walter, F., Brinks, E., & Kennicutt, R. C., Jr. 2008, AJ, 136, 2761

Oh, S.-H., de Blok, W. J. G., Brinks, E., Walter, F., & Kennicutt, R. C., Jr. 2011, AJ, 141, 193

Pontzen, A., & Governato, F. 2012, MNRAS, 421, 3464

Ragone-Figueroa, C., Granato, G. L., & Abadi, M. G. 2012, MNRAS, 3092

Read, J. I., & Gilmore, G. 2005, MNRAS, 356, 107

Reed, D., Governato, F., Verde, L., et al. 2005, MNRAS, 357, 82

Silich, S., & Tenorio-Tagle, G. 2001, ApJ, 552, 91

Spekkens, K., Giovanelli, R., & Haynes, M. P. 2005, AJ, 129, 2119

Spergel, D. N., Bean, R., Doré, O., et al. 2007, ApJS, 170, 377

Stadel, J., Potter, D., Moore, B., et al. 2009, MNRAS, 398, L21

Stinson, G. S., Dalcanton, J. J., Quinn, T., Kaufmann, T., & Wadsley, J. 2007, ApJ, 667, 170

Swaters, R. A., Madore, B. F., van den Bosch, F. C., & Balcells, M. 2003, ApJ, 583, 732

Tolstoy, E., Hill, V., & Tosi, M. 2009, ARA&A, 47, 371

Weinberg, M. D., & Katz, N. 2002, ApJ, 580, 627

Weisz, D. R., Dalcanton, J. J., Williams, B. F., et al. 2011, ApJ, 739, 5

Weldrake, D. T. F., de Blok, W. J. G., & Walter, F. 2003, MNRAS, 340, 12

Widrow, L. M. 2000, ApJS, 131, 39

Yoshii, Y., & Arimoto, N. 1987, A&A, 188, 13

Yoshii, Y., & Arimoto, N. 1991, A&A, 248, 30